Atmos. Chem. Phys. Discuss., 13, 32327–32351, 2013
www.atmos-chem-phys-discuss.net/13/32327/2013/
doi:10.5194/acpd-13-32327-2013

Atmospheric Chemistry and Physics
Discussions
Open Access

Local impact of solar variation on NO_2 in the lower mesosphere and upper stratosphere from 2007–2011

F. Friederich[1], **M. Sinnhuber**[1], **B. Funke**[2], **T. von Clarmann**[1], **and J. Orphal**[1]

[1]Karlsruhe Institute of Technology, Institute for Meteorology and Climate Research, Karlsruhe, Germany
[2]Instituto de Astrofísica de Andalucía, CSIC, Granada, Spain

Received: 18 October 2013 – Accepted: 26 November 2013 – Published: 10 December 2013

Correspondence to: F. Friederich (felix.friederich@kit.edu)

Published by Copernicus Publications on behalf of the European Geosciences Union.

Abstract

MIPAS/ENVISAT data of nighttime NO_2 volume mixing ratios (VMR) from 2007 until 2011 between 40 km and 62 km altitude are compared with the geomagnetic Ap index and solar Lyman α radiation. The local impact of variations in geomagnetic activity and solar radiation on the VMR of NO_2 in the lower mesosphere and upper stratosphere in the Northern Hemisphere is investigated by means of superposed epoch analysis. Observations show a clear 27 day period of the NO_2 VMR. This is positively correlated to the geomagnetic Ap index at 60–70° N geomagnetic latitude but also partially correlated to the solar Lyman α radiation. However, the dependency of NO_2 VMR on geomagnetic activity can be distinguished from the impact of solar radiation. This indicates a direct response of NO_x ($NO + NO_2$) to geomagnetic activity, probably due to precipitating particles. The response is detected in the range between 46 km and 52 km altitude. The NO_2 VMR epoch maxima due to geomagnetic activity is altitude-dependent and can reach up to 0.4 ppb, leading to mean production rates of 0.029 ppb (Ap d)$^{-1}$. This is the first study showing the local impact of electron precipitation on trace gases at that altitudes in the spring/summer/autumn hemisphere.

1 Introduction

Electrons of the aurora and the radiation belts can precipitate into the thermosphere, mesosphere, and even down to the upper stratosphere (Berger et al., 1970; Fang et al., 2008; Clilverd et al., 2010). They need relativistic energies to intrude into the lower mesosphere/upper stratosphere (Turunen et al., 2009). Precipitating electrons can ionize or dissociate atmospheric N_2, and subsequent (ion-)chemical reactions lead to an effective NO_x production (Porter et al., 1976; Rusch et al., 1981; Sinnhuber et al., 2012).

Auroral NO-production is well known in the thermosphere (e.g., Siskind et al., 1989), whereas the significance of NO_x-production due to electron precipitation in the meso-

ACPD
13, 32327–32351, 2013

sphere and stratosphere is still unclear. Renard et al. (2006) found an increase in stratospheric NO_2 in January–April 2004, supposing that the origin is caused by magnetospheric electrons, but Funke et al. (2007) showed that wintertime downward transport of thermospheric air was the more likely cause of NO_x enhancement in this case. Clilverd et al. (2009) showed a significant response of NO_2 VMR at 45–70 km altitude at high Northern latitudes to electron flux data in February 2004. However, also in this case it is unclear, to what extent wintertime downward transport has lead to the observed NO_x increase. Newnham et al. (2011) showed a direct nitric oxide response above 70 km due to electron precipitation. But still, a direct response of NO_x below 70 km altitude due to electron precipitation in the spring/summer/autumn hemisphere, where NO_x increases cannot be attributed to subsidence, has not been observed to our knowledge. Thus, it is unclear how much NO_x is produced directly in the mesosphere and upper stratosphere by electrons. An indirect indication of potential NO_x production, however, might be derived from Verronen et al. (2011) and Andersson et al. (2012), who showed a direct hydroxyl response to electron flux above 50 km.

A major influence on stratospheric and mesospheric NO_x is given by so-called solar proton events (SPE) (Crutzen et al., 1975; Jackman et al., 1980). Proton precipitation leads to an effective NO_x-production and can significantly enhance the VMR, e.g., about 50–60 ppb in the lower mesosphere in October–November 2003 (Jackman et al., 2005; López-Puertas et al., 2005).

The NO_x dependency on the solar spectral irradiance variabilities in the upper stratosphere/lower mesosphere has been investigated rarely to our knowledge. Keating et al. (1986) observed a response to the 27 day solar rotation signal in NO_2 at low latitudes below 40 km altitude. Hood et al. (2006) found a negative dependency of NO_x-anomalies on the Mg II solar UV index at the equatorial stratopause, and a positive dependeny at high latitudes at the upper stratosphere and the lower mesosphere using a 12 year data set of the Halogen Occultation Experiment (HALOE). Gruzdev et al. (2009) have searched for the 27 day solar rotation signal in NO and NO_2 by means of a 3-D Chemistry-Climate Model study. They have found significant sensitivities below

40 km and above 60 km, but not in between, although a connection with temperature and ozone both depending on solar UV radiation at these altitudes (Austin et al., 2007; Gruzdev et al., 2009) seems plausible.

In this study we analyze NO_2, which is the main constituent of NO_x in the upper stratosphere and lower mesosphere during night. For that, we use nighttime data of the nominal mode observations of the Michelson Interferometer for Passive Atmospheric Sounding (MIPAS, Fischer et al., 2008) on the Environmental Satellite (ENVISAT). We use the Ap index provided by the National Geophysical Data Center (http://www.ngdc.noaa.gov) as an indicator for geomagnetic activity, and Lyman α, provided by the LASP Interactive Solar Irradiance Data Center (LISIRD, http://lasp.colorado.edu/lisird/), as an indicator for solar UV radiation.

2 MIPAS/ENVISAT

Until contact was lost to ENVISAT on 08 April 2012, the MIPAS instrument recorded limb emission spectra of the Earth's atmosphere. Since spring 2002, MIPAS detected many atmospheric trace gases in the infrared region (4.1–14.7 µm) including NO_2 by its fundamental ν_3 band (6.2 µm). Due to the sun-synchronous orbit of ENVISAT, MIPAS measured at ~ 10 a.m. and ~ 10 p.m. local time. We use nighttime data (solar zenith angle > 96°) of the nominal measurement mode (6–68 km). Data are retrieved by the IMK-IAA processor (von Clarmann et al., 2003). The NO_2-retrieval is described in Funke et al. (2005) and has been improved since then (Funke et al., 2011). We use daily means of the versions V5R_NO2_220 and V5R_NO2_221. The arithmetic mean of the averaging kernel diagonal elements of single observations has to be greater than 0.03, in order to take the daily means of NO_2 into account.

ACPD
13, 32327–32351, 2013

3 Data analysis

In this section, we give a short overview about the data we use and the methods of data analysis (Sect. 3.1). We use the superposed epoch analysis method (SEA, Chree et al., 1913), also known as the compositing method (von Storch and Zwiers, 2001), to search for small responses to solar variations. We did SEAs with four different conditions in order to distinguish between the dependence on geomagnetic activity and solar UV radiation (Sect. 3.2). We analyze the SEAs by means of the Pearson correlation coefficient r to determine linear dependencies, and the quadrant correlation (Blomqvist et al., 1950) to determine non-linear, monotone dependencies. Finally, linear least-square fits to the SEAs lead to the determination of the altitude-dependent NO_x-lifetime, and the altitude- and Ap-index-dependent NO_x-production rate (Sect. 3.3).

3.1 Method

Figure 1 shows the daily zonal means of nighttime NO_2 VMR measured by MIPAS at $65\pm5^\circ$ N geomagnetic latitude, the Ap index, and solar Lyman α flux in 2007–2011, i.e., during solar minimum, as a function of time. Days for analysis were chosen such that the influence of other effects besides solar variabilities, e.g., due to NO_x subsidence in polar winter, is minimized in the Northern Hemisphere. There was no SPE affecting the Earth's atmosphere in the years 2007–2009, but one SPE occurred in 2010, and six SPEs in 2011 (http://www.swpc.noaa.gov). For each SPE the days from the onset until three days after the maximum are excluded. However, this was found to have no significant effect on the results of the paper.

At the chosen time periods over exactly 1000 days (Table 1), 659 daily means of MIPAS NO_2 VMR can be used. We restrict our analysis to geomagnetic latitudes from 50° S to 80° N for following reasons: first, with this restriction, downwelling of NO_x-rich upper atmospheric air in Southern polar winter is excluded. Second, because we analyze nighttime data, and our time periods include polar day at high Northern latitudes, there is not sufficient data at geomagnetic latitudes higher than 80° N. We analyze

ACPD
13, 32327–32351, 2013

10°-zonal means, restricting our analysis to Northern spring/summer/autumn because geomagnetic latitudes can be determined in the Northern Hemisphere more precisely than in the Southern Hemisphere.

A direct correlation of the Ap index and NO_2 VMR does not lead to a significant result. First, this is due to the predominance of the seasonal variability of NO_2. Further, only NO_2 anomalies can be unambiguously assigned to electron fluxes (or UV radiation), because constant electron-induced NO_x-production leads to an equilibrium concentration without rapid time dependence. Mid- and long-term variations compete against photochemistry and dynamics and are thus unaccessible to our analysis. Hence, a high-pass filter is applied to NO_2 VMR, Ap index, and Ly α as outlined in the following.

We assume that the measured NO_2 VMR is composed of two parts: The time-dependent $NO_{2_{\text{background}}}$ VMR which takes mid- and long-term variations into account, and changes due to short-time variabilities, $\Delta\,NO_2$. $NO_{2_{\text{background}}}$ is determined by a 27 day running mean representing a rectangular filter, shown as a red curve in Fig. 1 (top). In the same way, we determine variabilities of geomagnetic activity and solar radiation, i.e., $X = (NO_2, \text{Ap}, \text{Ly}\,\alpha)$:

$$\Delta X = X_{\text{measured}} - X_{\text{background}}. \quad (1)$$

To show similarities in the short-term behavior of $\Delta\,NO_2$, Δ Ap and Δ Ly α, we use the superposed epoch analysis (SEA) method, introduced by Chree et al. (1913), also known as the compositing method (von Storch and Zwiers, 2001). We define four classes of epochs. Each epoch is a time interval of ±30 days around day d. Days are considered, when Ap index and/or solar Ly α-fluxes fulfill particular conditions on day d as specified below. Further, only days are considered where MIPAS NO_2 nighttime measurements are available.

Epoch type 1. Δ Ap > 3.5 (shown by the red curve in Fig. 1, middle), to see the correlation between the signals of $\Delta\,NO_2$ and Δ Ap.

ACPD
13, 32327–32351, 2013

Epoch type 2. $\Delta\,\mathrm{Ap} > 3.5$ and $|\Delta\,\mathrm{Ly}\,\alpha| < 0.015\,\mathrm{photons\,cm^{-2}\,s^{-1}}$, in order to exclude UV radiation as a source of NO_x-variation from epoch type 1.

Epoch type 3. $\Delta\,\mathrm{Ly}\,\alpha > 0.05 \times 10^{11}\,\mathrm{photons\,cm^{-2}\,s^{-1}}$ (shown by the red curve in Fig. 1, bottom), to see the correlation between the signals of $\Delta\,NO_2$ and $\Delta\,\mathrm{Ly}\,\alpha$.

Epoch type 4. $\Delta\,\mathrm{Ly}\,\alpha > 0.05 \times 10^{11}\,\mathrm{photons\,cm^{-2}\,s^{-1}}$ and $|\Delta\,\mathrm{Ap}| < 1.0$, in order to exclude particle precipitation as a source of NO_x-production from epoch type 3.

Events at the day d are defined by the variations of the Ap index/solar Lyman α flux and not by their absolute values for the following reasons. First, a fixed threshold cannot define each single event in a 5 yr period due to long term-variations of the indices. Second, short-time variations in NO_2 are supposed to occur with short-time variations of the indices rather than exceeding a threshold with only little change in the absolute value due to mid- or long-term variations. These are in competition with photochemistry and dynamics and not verifiable with the SEA.

The thresholds are chosen in this way, that on the one hand the sample of events/epochs is sufficiently large, on the other hand as high as possible. We obtain the following number of events $N = 103/34/96/21$ for epoch type 1/2/3/4, respectively. These N time series of the quantities $q = (\Delta\,NO_2, \Delta\,\mathrm{Ap}, \Delta\,\mathrm{Ly}\,\alpha)$, each 61 days long, are co-added

$$\overline{q}_i = \frac{\sum_{j=1}^{M_i} q_{i,j}}{M_i}, i = [1,61], \qquad (2)$$

i.e., averaged under consideration of their phase with respect to the $\Delta\,\mathrm{Ap}/\Delta\,\mathrm{Ly}\,\alpha$ event, which is called SEA. Due to gaps in the time series of NO_2 VMR, the number of summands M_i at each phase point i is lower than the number of epochs N (roughly $M_i \simeq 0.7 \cdot N$).

ACPD
13, 32327–32351, 2013

3.2 Different epoch types

The SEA is exemplified in Fig. 2 as a black curve at 50 km altitude and 65 ± 5° N geomagnetic latitude for ΔNO_2, Δ Ap, and Δ Ly α and for all four epoch types. The blue error bars show the 1σ standard error of the mean of each value in all figures. In the following, we describe the different epoch types in detail, for each starting with the conditions mentioned in Sect. 3.1.

Epoch type 1, Δ Ap > 3.5, $N = 103$: There are sharp peaks around the days −27, 1, and 28 at ΔNO_2, around the days −27, 0, and 27 at Δ Ap, and broad peaks at Δ Ly α with maxima on the same days. This is consistent with the average solar rotation. There is roughly the same peak value at the days −27, 0, and 27 at ΔNO_2 and Δ Ly α, but different peak values at Δ Ap. This together with the broadening of the ΔNO_2 peak indicates the influence of the UV radiation. There are distinct, but not significant small maxima between the days −27, 0, and 27. They are triggered by out-of-phase UV radiation having a non-linear influence on ΔNO_2, which is explained below.

Epoch type 2, Δ Ap > 3.5 and |Δ Ly α| < 0.015 photons cm^{-2} s^{-1}, $N = 34$: The significant correlation between Δ Ap and ΔNO_2 is more pronounced, if variations in Δ Ly α are suppressed. The 27-day-period is clearly visible. Here, the central peak at day 1 is even higher than those one period before and after. Evidently, the averaged NO_2 enhancement is caused by pure electron precipitation. The out-of-phase UV-radiation signal appears faintly at ΔNO_2 with a broad maximum around the day −10.

Epoch type 3, Δ Ly α > 0.05 × 10^{11} photons cm^{-2} s^{-1}, $N = 96$: There are broad peaks around the days −27, 0, and 27 at ΔNO_2, Δ Ap, and Δ Ly α and the correlation between Δ Ly α, and ΔNO_2 is noticeably good.

Epoch type 4, Δ Ly α > 0.05 × 10^{11} photons cm^{-2} s^{-1} and |Δ Ap| < 1.0, $N = 21$: The signal is not as smooth as in epoch type 3, due to the smaller N and due to a noisy Δ Ap signal. Both epoch types 3 and 4 show that changes in the UV flux have a significant impact on NO_2, probably triggered by the response of ozone and temperature to UV flux changes at these altitudes (e.g., Austin et al., 2007), throughout the 27 day cycle.

ACPD
13, 32327–32351, 2013

Thus, again, we have to consider the impact of UV radiation while searching for the one of particle precipitation.

As discussed above, in epoch type 2, only very small UV radiation variations are permitted. The correlation coefficient r of that epoch type between Δ Ap and ΔNO_2 is shown for all calculated altitudes and geomagnetic latitudes in Fig. 3. The three panels (top/middle/bottom) show the resultant r when the ΔNO_2 signal has a delay of 0/1/2 days, respectively. The correlation coefficient is highest (greater than 0.6) at geomagnetic latitudes of the outer radiation belt at $65 \pm 5^{\circ}$ N and one day delay. The central peak of the ΔNO_2 SEA appears also at day 1. There is no significant correlation at lower Northern or Southern geomagnetic latitudes.

We also calculated epoch type 2 for geographic zonal means. The correlation coefficients for a delay of one day in ΔNO_2, are shown in Fig. 4. They become significantly lower at high Northern latitudes. Consequently, Figs. 3 and 4 point out that the observed NO_x is dependent on high Northern geomagnetic latitudes and not on geographic latitudes. This is another hint for the local impact of electron precipitation.

Even though a dependence of ΔNO_2 on Δ Ly α is clearly visible in the SEA, linear dependency cannot be assumed due to several simultaneous influences. UV radiation has an impact on the temperature, ozone, the ozone column above, and on the NO photolysis rate, for example, each resulting in variations of the NO_2 VMR at night. Thus we need a method which is able to detect also nonlinear correlations. We have chosen the quadrant correlation (Blomqvist et al., 1950) which requires only that the relation between two variables is monotonic. Here, every daily mean is considered, subject to the condition that $|\Delta \mathrm{Ap}| < 1.0$ is true for the certain day and the day before.

In Fig. 5, the quadrant correlation is plotted over geomagnetic latitudes, in Fig. 6, respectively, over geographic latitudes. The color code shows both the precision p and the sign of the correlation. Figure 5 shows a positive correlation on $65 \pm 5^{\circ}$ N geomagnetic latitude which could be caused by electron precipitation in phase with solar Lyman α flux, not filtered out by the Ap index criterion. In Fig. 6, there is a strong correlation at 45–65° N and 48–50 km altitude. It could be partly a blurred effect of the positive correlation appearing in geomagnetic latitudes. But since p is even higher, simultaneous variations in temperature, ozone, and NO-photolysis affect ΔNO_2 as well, leading to a positive correlation at high latitudes and a negative correlation at lower latitudes.

However, the detailed analysis of the UV-radiation response is beyond the scope of the paper. In the following, it is only essential that the UV-radiation response does not affect the Ap response which is the case for epoch type 2.

3.3 Fit to the SEA

In order to determine an Ap index depending NO_x-production rate we fit a simple model to the epoch type 2-SEAs of ΔNO_2 at $65 \pm 5^\circ$ N geomagnetic latitude. We account for a linear dependency of the Ap index, namely the NO_x-production rate per day pr, and the altitude-dependent NO_x lifetime τ. Effects of the rectangular filter we use to determine $NO_{2_{\text{background}}}$ are insignificant. As a first step, we determine pr and τ iteratively by minimizing the residual:

$$\chi^2 = \sum_{i=0}^{60} \left(\frac{\sum_{t=0}^{T} e^{\frac{-t}{\tau}} \cdot \text{pr} \cdot \Delta \text{Ap}_{i-t} - \Delta \text{NO}_{2_i}}{\sigma_i} \right)^2 . \quad (3)$$

T denotes an integer depending on τ (typically $\sim 2-3 \cdot \tau$). σ_i denotes the variance of ΔNO_{2_i}. In Fig. 7 (right), τ is plotted in dependence on the altitude. At altitudes higher than 54 km, τ becomes most likely lower than one day. But the analysis of daily means is not able to resolve that. This is why the figure is shadowed at these altitudes. The ΔNO_2-lifetimes are significantly lower at all altitudes than the NO_x-lifetimes after a SPE determined by Friederich et al. (2013). τ is mostly triggered by dynamics at these altitudes (Brasseur and Solomon, 2005; Friederich et al., 2013). At a SPE, NO_x is enhanced over the whole polar cap, whereas NO_x enhancement due to electron precipitation is restricted to a small region. Due to mixing with air which was not affected by electron precipitation the dynamical lifetime of NO_x is significantly lower than after a SPE.

In order to determine pr precisely together with its variance, we applied a least squares fit utilizing τ determined before. In Fig. 7 (middle), pr is plotted with its 1σ range in dependence on altitude. The black curve shows the result for epoch type 1, the blue one for epoch type 2. The $\Delta\,NO_2$-value at day 1, hereinafter called sensitivity, of the epoch types 1/2/3 is shown as a black/blue/red curve, respectively, in the left column of Fig. 7.

Below 44 km there is neither any signal in the sensitivity nor in the production rate. Thus, 44 km is the lower boundary, where electron precipitation can be detected with NO_2 measurements of MIPAS in 2007–2011. The sensitivity maximizes at 48 km at 0.20/0.41 ppb for epoch type 1/2, respectively, while the production rate maximizes at 50 km at 0.015/0.029 ppb $(\mathrm{Ap\,d})^{-1}$. The difference in altitude can be explained by the different NO_x-lifetimes. At altitudes higher than 52 km there is neither any significant sensitivity nor any positive production rate. This is most probably due to the fact that the NO_x-lifetime is lower than one day making it impossible to detect it by analyzing daily means. Nevertheless, it should be considered that the NO_2/NO_x-ratio decreases with altitude at night. Additionally, the efficiency of NO_x production due to ionization, which is mainly influenced by temperature-dependent reactions, shows its peak between 42 km and 52 km (Funke et al., 2011; Friederich et al., 2013). These two reasons could also explain the decrease of the production rate from 50 km to 52 km. The fits of epoch type 2 are shown in Fig. 8 at 54/50/46 km altitude (top/middle/bottom, respectively).

4 Conclusions

We showed the significant influence of solar variabilities on nighttime NO_2 and consequently on NO_x in the lower mesosphere and upper stratosphere during solar minimum. The 27 day period is clearly visible in $\Delta\,NO_2$ generated by short-time variabilities in solar UV radiation and electron precipitation. We have distinguished the geomagnetic

ACPD
13, 32327–32351, 2013
Local impact of solar variation on mesospheric NO_2
F. Friederich et al.

influence from that of UV radiation at 60–70° N geomagnetic latitude. This distinction and the fact, that there is only a signal at geomagnetic latitudes of the outer radiation belt, lead to the conclusion, that electron precipitation is a source of NO_x-production in the lower mesosphere and upper stratosphere.

The MIPAS nighttime NO_2 signal shows a delay of one day to the Ap index. Likewise, other studies have shown a delay of one day of the auroral NO production compared to auroral activity between 100 km and 160 km (Solomon et al., 1999; Marsh et al., 2004). Newnham et al. (2011) see a 1–2 day delay of enhanced NO, with respect to the > 30 keV and > 300 keV electron flux at altitudes between 70 km and 85 km. Thus, the MIPAS NO_2 observations in the lower mesosphere and upper stratosphere are consistent with previous NO observations in the upper mesosphere and lower thermosphere but being of considerably lower magnitude.

The correlation coefficient r between the SEAs of Δ Ap and Δ NO_2 is greater than 0.4 between 44 km and 52 km altitude. Andersson et al. (2012) showed that the correlation coefficients of single events between daily mean OH and daily mean 100–300 keV electron count rates are greater than 0.35 down to 52 km. They did not find a clear correlation below. The NO_2 enhancement due to electron impact shown in this study is low but significant. Altitude-dependent production rates were determined maximizing at 0.029 ppb $(\mathrm{Ap\,d})^{-1}$ at 50 km altitude. Above, the decrease of the signal with altitude could be explained by a decrease of the nighttime NO_2/NO_x-ratio, with the efficiency of NO_x-production, and mainly with the altitude-dependent NO_x-lifetime.

This is the first study showing the independent influence of electron precipitation on NO_2, and on trace gases in general, at altitudes between 46 km and 52 km in the spring/summer/autumn hemisphere to our knowledge. Further studies are necessary to investigate the possible impact on ozone and examine the NO_x-production rates during solar maximum.

Acknowledgements. F. Friederich and M. Sinnhuber gratefully acknowledge funding by the Helmholtz Association of German Research Centres (HGF), grant VH-NG-624.

The service charges for this open access publication have been covered by a Research Centre of the Helmholtz Association.

References

Andersson, M. E., Verronen, P. T., Wang, S., Rodger, C. J., Clilverd, M. A., and Carson, B. R.: Precipitating radiation belt electrons and enhancements of mesospheric hydroxyl during 2004–2009, J. Geophys. Res., 117, D09304, doi:10.1029/2011JD017246, 2012. 32329, 32338

Austin, J., Hood, L. L., and Soukharev, B. E.: Solar cycle variations of stratospheric ozone and temperature in simulations of a coupled chemistry-climate model, Atmos. Chem. Phys., 7, 1693–1706, doi:10.5194/acp-7-1693-2007, 2007. 32330, 32334

Berger, M. J., Seltzer, S. M., and Maeda, K.: Energy deposition by auroral electrons in the atmosphere, J. Atmos. Terr. Phys., 32, 1015–1045, 1970. 32328

Blomqvist, N.: On a measure of dependence between two random variables, Ann. Math. Statist., 21, 593–601, 1950. 32331, 32335

Brasseur, G. P. and Solomon, S.: Aeronomy of the Middle Atmosphere, 3rd edn., Springer, Dordrecht, the Netherlands, 2005. 32336

Chree, C.: Some Phenomena of Sunspots and of Terrestrial Magnetism at Kew Observatory, Philos. T. Roy. Soc. London, 212, 75–116, 1913. 32331, 32332

Clilverd, M. A., Seppälä, A., Rodger, C. J., Mlynczak, M. G., and Kozyra, J. U.: Additional stratospheric NO_x production by relativistic electron precipitation during the 2004 spring NO_x descent event, J. Geophys. Res., 114, A04305, doi:10.1029/2008JA013472, 2009. 32329

Clilverd, M. A., Rodger, C. J., Gamble, R. J., Ulich, T., Raita, T., Seppälä, A., Green, J. C., Thomson, N. R., Sauvaud, J.-A., and Parrot, M.: Ground-based estimates of outer radiation belt energetic electron precipitation fluxes into the atmosphere, J. Geophys. Res., 115, A12304, doi:10.1029/2010JA015638, 2010. 32328

Crutzen, P. J., Isaksen, I. S. A., and Reid, G. C.: Solar proton events – stratospheric sources of nitric oxide, Science, 189, 457–459, doi:10.1126/science.189.4201.457, 1975. 32329

Fang, X., Randall, C. E., Lummerzheim, D., Solomon, S. C., Mills, M. J., Marsh, D. R., Jackmann, C. H., Wang, W., and Lu, G.: Electron impact ionization: A new parameterization for 100 eV to 1 MeV electrons, J. Geophys. Res., 113, A09311, doi:10.1029/2008JA013384, 2008. 32328

Fischer, H., Birk, M., Blom, C., Carli, B., Carlotti, M., von Clarmann, T., Delbouille, L., Dudhia, A., Ehhalt, D., Endemann, M., Flaud, J. M., Gessner, R., Kleinert, A., Koopman, R., Langen, J., López-Puertas, M., Mosner, P., Nett, H., Oelhaf, H., Perron, G., Remedios, J., Ridolfi, M., Stiller, G., and Zander, R.: MIPAS: an instrument for atmospheric and climate research, Atmos. Chem. Phys., 8, 2151–2188, doi:10.5194/acp-8-2151-2008, 2008. 32330

Friederich, F., von Clarmann, T., Funke, B., Nieder, H., Orphal, J., Sinnhuber, M., Stiller, G. P., and Wissing, J. M.: Lifetime and production rate of NO_x in the upper stratosphere and lower mesosphere in the polar spring/summer after the solar proton event in October–November 2003, Atmos. Chem. Phys., 13, 2531–2539, doi:10.5194/acp-13-2531-2013, 2013. 32336, 32337

Funke, B., López-Puertas, M., von Clarmann, T., Stiller, G. P., Fischer, H., Glatthor, N., Grabowski, U., Höpfner, M., Kellmann, S., Kiefer, M., Linden, A., Mengistu Tsidu, G., Miliz, M., Steck, T., and Wang, D. Y.: Retrieval of stratospheric NO_x from 5.3 and 6.2 μm nonlocal thermodynamic equilibrium emissions measured by Michelson Interferometer for Passive Atmospheric Sounding (MIPAS) on Envisat, J. Geophys. Res., 110, D09302, doi:10.1029/2004JD005225, 2005. 32330

Funke, B., López-Puertas, M., Fischer, H., Stiller, G. P., von Clarmann, T., Wetzel, G., Carli, B., and Belotti, C.: Comment on "Origin of the January–April 2004 increase in stratospheric NO_2 observed in the northern polar latitudes", Geophys. Res. Lett., 34, L07813, doi:10.1029/2006GL027518, 2007. 32329

Funke, B., Baumgaertner, A., Calisto, M., Egorova, T., Jackman, C. H., Kieser, J., Krivolutsky, A., López-Puertas, M., Marsh, D. R., Reddmann, T., Rozanov, E., Salmi, S.-M., Sinnhuber, M., Stiller, G. P., Verronen, P. T., Versick, S., von Clarmann, T., Vyushkova, T. Y., Wieters, N., and Wissing, J. M.: Composition changes after the "Halloween" solar proton event: the High Energy Particle Precipitation in the Atmosphere (HEPPA) model versus MIPAS data intercomparison study, Atmos. Chem. Phys., 11, 9089–9139, doi:10.5194/acp-11-9089-2011, 2011. 32330, 32337

Gruzdev, A. N., Schmidt, H., and Brasseur, G. P.: The effect of the solar rotational irradiance variation on the middle and upper atmosphere calculated by a three-dimensional chemistry-climate model, Atmos. Chem. Phys., 9, 595–614, doi:10.5194/acp-9-595-2009, 2009. 32329, 32330

Jackman, C. H., Frederick, J. E., and Stolarski, R. S.: Production of odd nitrogen in the stratosphere and mesosphere: An intercomparison of source strengths, J. Geophys. Res., 85, 7495–7505, doi:10.1029/JC085iC12p07495, 1980. 32329

Jackman, C. H., DeLand, M. T., Labow, G. J., Fleming, E. L., Weisenstein, D. K., Ko, M. K. W., Sinnhuber, M., and Russell, J. M.: Neutral atmospheric influences of the solar proton events in October–November 2003, J. Geophys. Res., 110, A09S27, doi:10.1029/2004JA010888, 2005. 32329

Hood, L. L. and Soukharev, B. E.: Solar induced variations of odd nitrogen: Multiple regression analysis of UARS HALOE data, J. Res. Lett., 33, L22805, doi:10.1029/2006GL028122, 2006. 32329

Keating, G. M., Nicholson III, J., Brasseur, G., De Rudder, A., Schmailzl, U., and Pitts, M.: Detection of stratospheric HNO_3 and NO_2 response to short-term solar ultraviolet variability, Nature, 322, 43–46, doi:10.1038/322043, 1986. 32329

López-Puertas, M., Funke, B., Gil-López, S., von Clarmann, T., Stiller, G. P., Höpfner, M., Kellmann, S., Fischer, H., and Jackson, C. H.: Observations of NO_x-Enhancements and Ozone Depletion in the Northern and Southern Hemispheres after the October-November 2003 Solar Proton Events, J. Geophys. Res., 110, A09S44, doi:10.29/2005JA011051, 2005. 32329

Marsh, D. R., Solomon, S. C., and Reynolds, A. E.: Empirical model of nitric oxide in the lower thermosphere, J. Geophys. Res., 109, A07301, doi:10.1029/2003JA010199, 2004. 32338

Newnham, D. A., Espy, P. J., Clilverd, M. A., Rodger, C. J., Seppälä, A., Maxfield, D. J., Hartogh, P., Holmén, K., and Horne, R. B.: Direct observations of nitric oxide produced by energetic electron precipitation into the Antarctic middle atmosphere, Geophys. Res. Lett., 38, L20104, doi:10.1029/2011GL048666, 2011. 32329, 32338

Porter, H. S., Jackman, C. H., and Green, A. E. S.: Efficiencies for production of atomic nitrogen and oxygen by relativistic proton impact in air, J. Chem. Phys., 65, 154–167, 1976. 32328

Renard, J.-B., Blelly, P.-L., Bourgeois, Q., Chartier, M., Goutail, F., and Orsolini, Y. J.: Origin of the January – April 2004 increase in stratospheric NO_2 observed in the northern polar latitudes, Geophys. Res. Lett., 33, doi:10.1029/2005GL025450, 2006. 32329

Rusch, D. W., Gerard, J.-C., Solomon, S., Crutzen, P. J., and Reid, G. C.: The effect of particle precipitation events on the neutral and ion chemistry of the middle atmosphere, 1. Odd nitrogen, Planet. Space Sci., 29, 767–774, 1981. 32328

ACPD

13, 32327–32351, 2013

Title Page
Abstract Introduction
Conclusions References
Tables Figures
◀ ▶
Back Close
Full Screen / Esc
Printer-friendly Version
Interactive Discussion

Sinnhuber, M., Nieder, H., and Wieters, N.: Energetic Particle Precipitation and the Chemistry of the Mesosphere/Lower Thermosphere, Surv. Geophys., Springer Netherlands, Dordrecht, doi:10.1007/s10712-9201-3, 2012. 32328

Siskind, D., Barth, C. A., and Roble, R.: The response of thermospheric nitric oxide to an auroral storm, 2. Auroral latitudes, J. Geophys. Res., 94, 16899–16911, doi:10.1029/JA094iA12p16899, 1989. 32328

Solomon, S. C., Barth, C. A., and Bailey, S. M.: Auroral production of nitric oxide measured by the SNOE satellite, Geophys. Res. Lett., 26, 1259–1262, 1999. 32338

Turunen, E., Verronen, P. T., Seppälä, A., Rodger, C. J., Cliverd, M. A., Tamminen, J., Enell, C.-F., and Ulich, T.: Impact of different energies of precipitating particles on NO_x generation in the middle and upper atmosphere during geomagnetic storms, J. Atmos. Sol. Terr. Phys., 71, 1176–1189, doi:10.1016/j.jastp.2008.07.005, 2009. 32328

Verronen, P. T., Rodger, C. J., Cliverd, M. A., and Wang, S.: First evidence of mesospheric hydroxyl response to electron precipitation from the radiation belts, J. Geophys. Res., 116, D07307, doi:10.1029/2011JD014965, 2011. 32329

von Clarmann, T., Glatthor, N., Grabowski, U., Höpfner, M., Kellmann, S., Kiefer, M., Linden, A., Mengistu Tsidu, G., Milz, M., Steck, T., Stiller, G. P., Wang, D. Y., Fischer, H., Funke, B., Gil López, S., and López-Puertas, M.: Retrieval of temperature and tangent altitude pointing from limb emission spectra recorded from space by the Michelson Interferometer for Passive Atmospheric Sounding (MIPAS), J. Geophys. Res., 108, 4736, doi:10.1029/2003JD003602, 2003. 32330

von Storch, H. and Zwiers, F. W.: Statistical Analysis in Climate Research, Cambridge Univ. Press, Cambridge, UK, 2001. 32331, 32332

ACPD
13, 32327–32351, 2013

Local impact of solar variation on mesospheric NO_2

F. Friederich et al.

Table 1. Time periods, for which MIPAS NO_2 data are used in the analysis.

year	selected days
2007	21 Mar–28 Oct
2008	5 Apr–5 Oct
2009	28 Apr–7 Oct
2010	20 Mar–12 Oct
2011	24 Feb–5 Oct

ACPD
13, 32327–32351, 2013

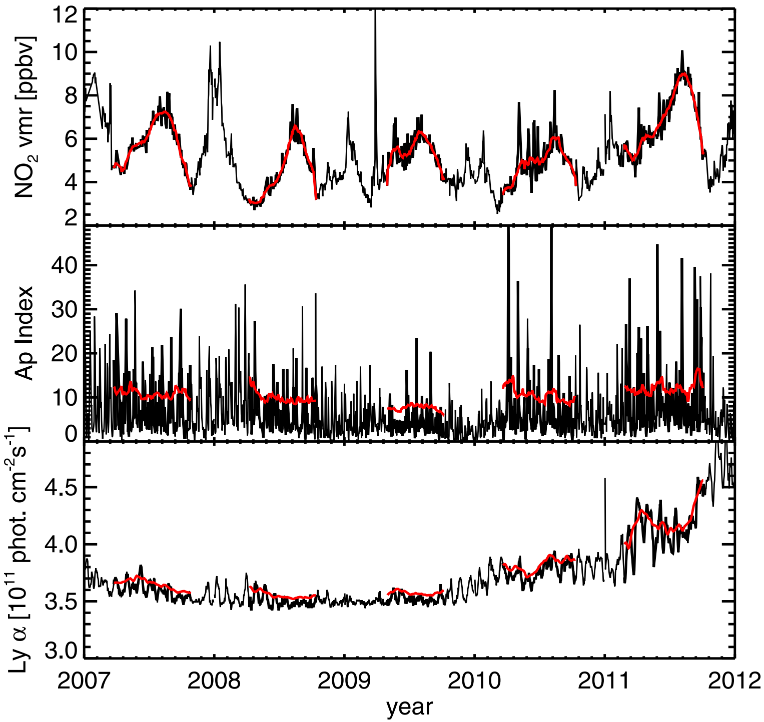

Fig. 1. Top: Daily means of nighttime NO_2 VMR in ppb at $65 \pm 5^\circ$ N geomagnetic latitude and 50 km altitude in 2007–2011. The red curve shows the 27 day running mean of the curve for the days listed in Table 1. Middle: Daily means of the Ap index in 2007–2011. The red curve shows the 27 day running mean of the curve shifted by 3.5 for the days listed in Table 1 defining the threshold of an Δ Ap-event. Bottom: Solar Lyman α in 2007–2011. The red curve shows the 27 day running mean of the curve shifted by 0.05 photons $cm^{-2}\,s^{-1}$ for the days listed in Table 1 defining the threshold of an Δ Lyman α-event.

ACPD
13, 32327–32351, 2013

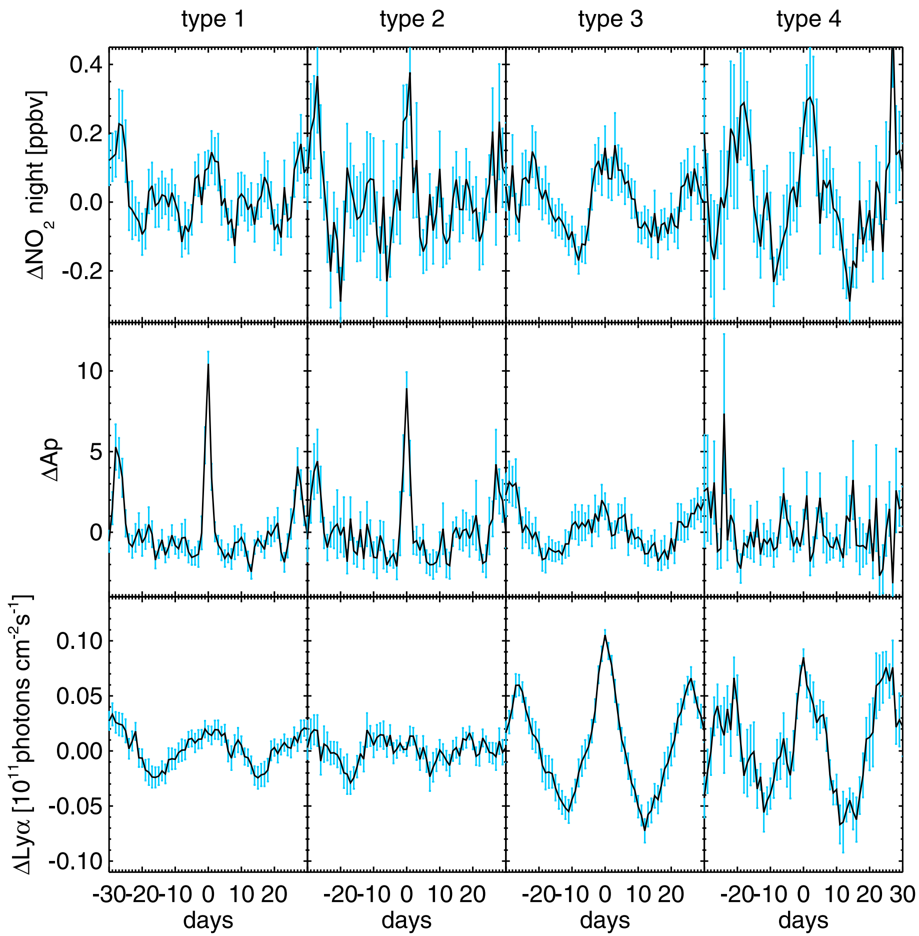

Fig. 2. SEAs of 103/34/96/21 (epoch type 1/2/3/4, respectively) different events in 2007–2011 at 50 km altitude and 65 ± 5° N geomagnetic latitude. The columns define the epoch type number, the rows show Δ NO_2, Δ Ap, and Δ Ly α.The blue error bars show the 1σ range.

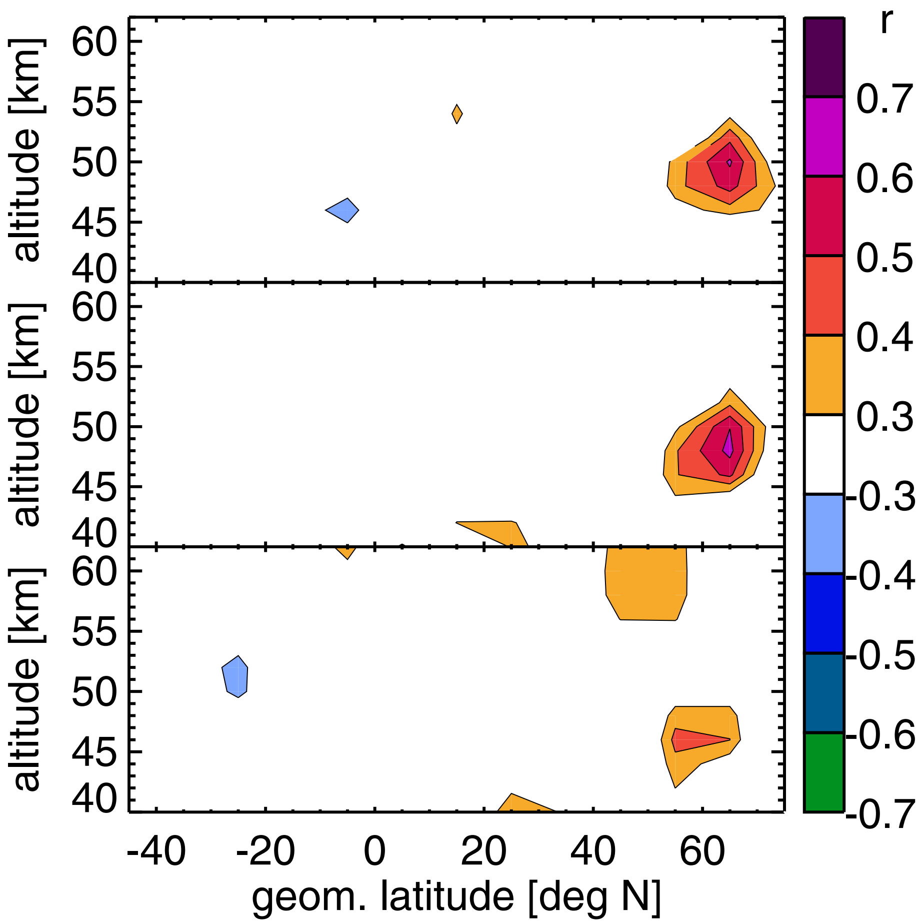

Fig. 3. Correlation coefficient *r* of the SEA with respect to Δ Ap (epoch type 2) between Δ Ap and ΔNO_2, plotted over geomagnetic latitudes with 0/1/2 days delay (top/middle/bottom, respectively).

ACPD
13, 32327–32351, 2013

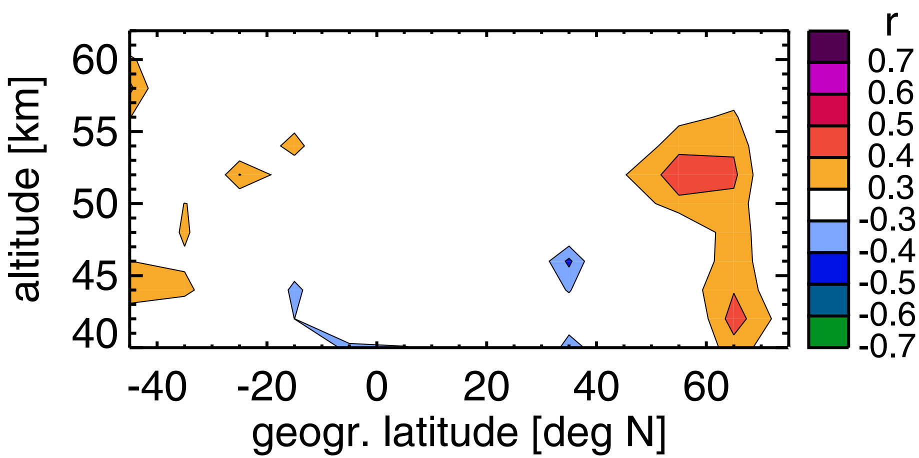

Fig. 4. Correlation coefficient *r* of the SEA with respect to Δ Ap (epoch type 2) between Δ Ap and Δ NO_2 with a delay of one day, plotted over geographic latitudes.

ACPD
13, 32327–32351, 2013

Local impact of solar variation on mesospheric NO_2

F. Friederich et al.

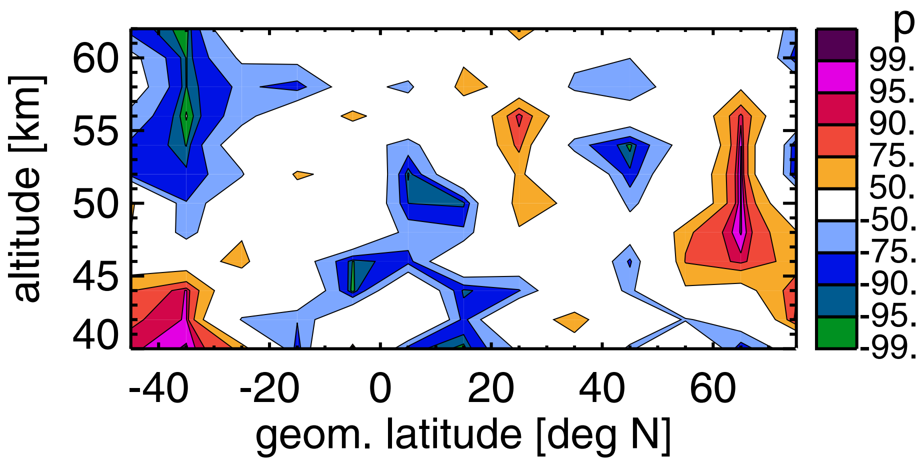

Fig. 5. Altitude- and geomagnetic latitude-dependent precision p of the quadrant correlation of Δ Ly α and Δ NO_2. The sign indicates whether the correlation is positive or negative.

ACPD
13, 32327–32351, 2013

Local impact of solar variation on mesospheric NO_2

F. Friederich et al.

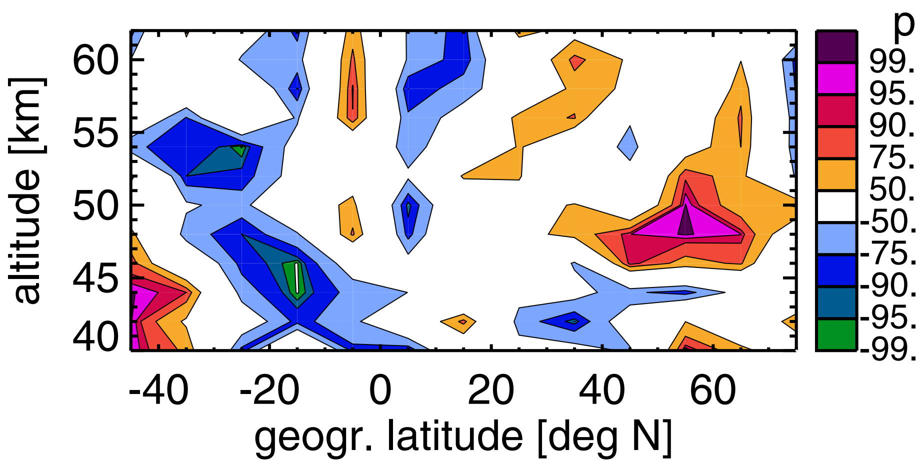

Fig. 6. Same as Fig. 5 but with geographic latitudes.

ACPD
13, 32327–32351, 2013

Local impact of solar variation on mesospheric NO_2

F. Friederich et al.

Title Page
Abstract
Introduction
Conclusions
References
Tables
Figures
◀◀
▶▶
◀
▶
Back
Close
Full Screen / Esc
Printer-friendly Version
Interactive Discussion

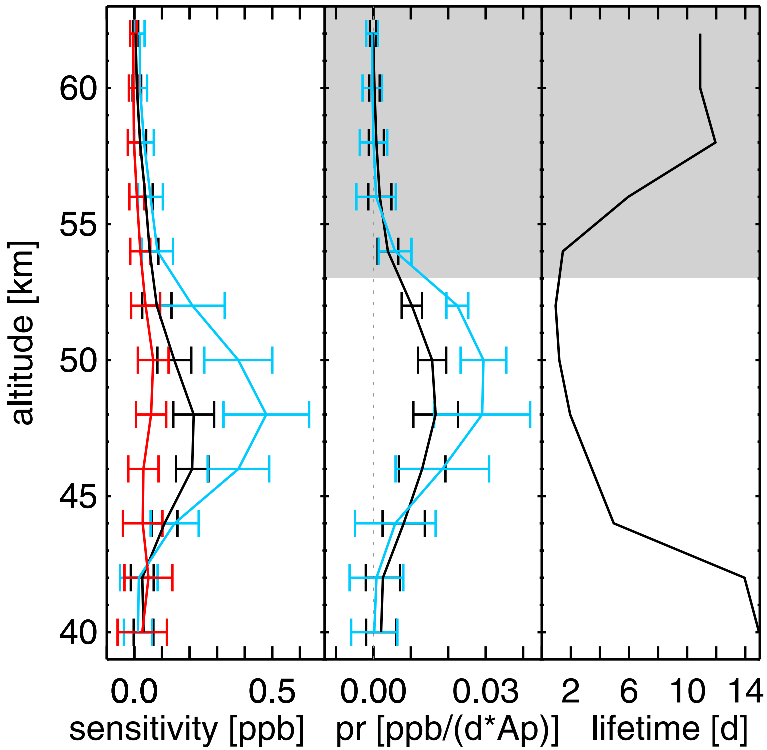

Fig. 7. Left: Altitude dependent sensintivity of ΔNO_2 on the conditions of epoch type 1/2/3 shown in black/blue/red, respectively. Middle: Altitude-dependent production rate pr or epoch type 1/2 shown in black/blue, respectively. Right: Altitude-dependent ΔNO_2-lifetime at night. All quantities were determined at $65 \pm 5^\circ$ N geomagnetic latitude. The error bars show the 1σ range. The shadowed area marks the altitudes, where the determination of the lifetime is not reliable.

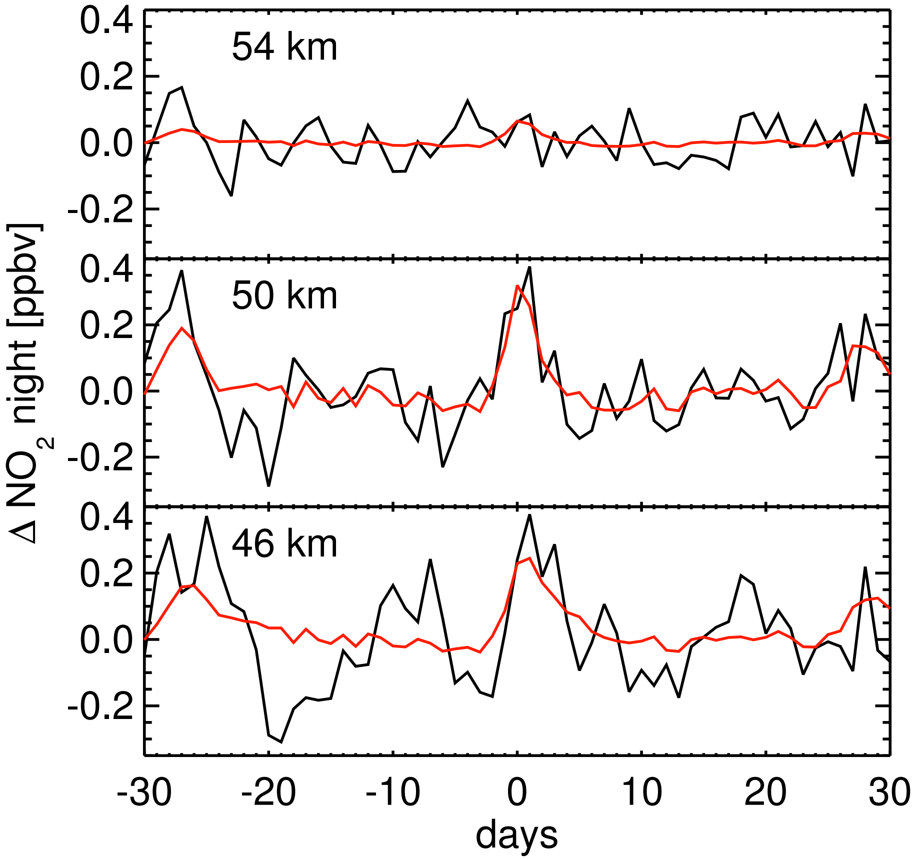

Fig. 8. SEA of Δ NO_2 at $65 \pm 5^\circ$ N geomagnetic latitude and different altitudes (black). In red the corresponding fits.

ACPD
13, 32327–32351, 2013

Local impact of solar variation on mesospheric NO_2

F. Friederich et al.